Research Square

Preprints are preliminary reports that have not undergone peer review.
They should not be considered conclusive, used to inform clinical practice,
or referenced by the media as validated information.

Deterministic projection selection for Limited-View Computed Tomography

Munnu Sonkar

munnu.sonkar@nitkkr.ac.in

National Institute of Technology

Pradip Sasmal

Indian Institute of Technology Jodhpur

CS Sastry

Indian Institute of Technology Hyderabad

Research Article

Keywords: Non-negative sparse signal recovery, Radon projection matrix, Unit norm tight frame, Block sparse solver, Limited-view tomography

Posted Date: November 17th, 2026

DOI: https://doi.org/10.21203/rs.3.rs-8662735/v1

License: This work is licensed under a Creative Commons Attribution 4.0 International License.
Read Full License

Additional Declarations: No competing interests reported.

Deterministic projection selection for Limited-View Computed Tomography

Munnu Sonkar[a,1,⋆], **Pradip Sasmal**[b,2], **CS Sastry**[b,3]

[1] Department of Mathematics, National Institute of Technology, Kurukshetra, 136119 India.
[2]Department of Mathematics, Indian Institute of Technology Jodhpur, 342037, India.
[3]Department of Mathematics, Indian Institute of Technology Hyderabad, 502285, India.

Received: date / Accepted: date

Abstract In Limited-View Computed Tomography (LVCT), one restricts the number of projection angles (or views) for data reduction, which has many implications, especially in medical domain. In most of the existing works on LVCT, the views are sampled randomly or in equi-spaced manner, which makes the sampling process oblivion to the image reconstruction solvers. Motivated by this gap between the sampling strategy and the image reconstruction solvers, we propose a deterministic way of finding an optimal set of views for LVCT using block-sparse optimization problem. The proposed methodology is tied to a selection of Radon sub-matrix possessing low total coherence which is desired for sparsity-based CT image reconstruction. We demonstrate efficacy of the proposed deterministic LVCT in recovering CT images.

Keywords Non-negative sparse signal recovery, Radon projection matrix, Unit norm tight frame, Block sparse solver, Limited-view tomography.

1 Introduction

Limited-view computed tomography (LVCT) examines an object's internal structure using a limited number of projections, which correspond to some of the angles. By limiting the number of projections, LVCT significantly decreases radiation exposure, thereby decreasing the associated cancer risk. The view restricted problem results in an underdetermined system of linear equations, making the problem incomplete, ill-posed, and generally ill-conditioned. Several researchers [14, 22, 31, 32] have shown that proper choice of the projection angles for reconstruction solvers can particularly be crucial when only a limited number of projections are available. The authors [22, 31, 32] have considered various sampling strategies for selecting projection angles, such as random and equiangular, which are independent of the reconstruction solvers. They have demonstrated that the choice of projection angles significantly impacts quality in reconstruction of binary images (typically 0 and 1) for specific solvers. The authors of [31] have used the *Difference of Convex* (DC) algorithm [25], while others [22] have employed the simulated annealing (SA) optimization [12] procedure to reconstruct underlying images.

The area of compressive sensing (CS) has recently emerged as an alternative source of methods that can be used very effectively for applications in CT [8, 10, 26, 34]. Notwithstanding the greater relevance of CS to applications in CT, there is still a loose-end in the literature, which is explained through an example now. When a CS-based solver is executed on different restricted sets of projection views as shown in Table 1, one obtains the reconstructions as shown in Figure 3. The differences in the quality of the reconstruction indicate that the recovery quality for the five sets is highly dependent on the choice of angles. In particular, in the cases of the first 4 sets of projection angles (taken independently of the reconstruction solver), the image reconstruction solvers are completely oblivion, resulting in below-par quality. In the case of the fifth set of angular views, which is tied to the reconstruction solver (explained in more detail in a later section), the reconstruction quality is much superior. Motivated by this observation and the gap between reconstruction solvers and the sampling strategies of projection angles, the present work aims to link the subsampling of projection angles in LVCT to the reconstruction solvers. We realize our objective of deterministic selection of optimal-projection-angles by proposing a block-sparse based optimization problem. In CS theory, block-

⋆Corresponding Author
[a]munnu.sonkar@nit.ac.in
[b]psasmal@iitj.ac.in
[c]csastry@math.iith.ac.in

based solvers have gained prominence [5] as they obtain the solutions possessing a certain block structure. Viewing the Radon sensing matrix as a block matrix, with each block standing for one view, we propose a non-negative block-sparse recovery method whose solution leads to the optimal Radon sub-matrix for LVCT. This matrix being optimal in the sense of sparse recovery properties is expected to provide a reconstruction of optimal quality when sparse reconstruction methods are used. To the best of our knowledge, this is first of a kind result that connects sampling of projection angles in LVCT to reconstruction solvers. The contributions of the present work are summarised below:

- Determining the optimal set of angular parameters for LVCT from a mathematical problem based on the sparse recovery properties (SRPs) of the underlying Radon matrix. Translating, subsequently, the selection of optimal views for LVCT to a block-sparse signal recovery problem, which links the sampling-strategy to the reconstruction solvers.
- Demonstrating empirically that the sensing matrix corresponding to the proposed deterministic-LVCT possesses better sparse recovery properties such as lower total coherence (which is defined in Section 2.1) compared to its random-LVCT counterpart. Consequently, the deterministic sensing matrix exhibits reconstruction of better quality.

The paper is organized as several sections. We present in Section 2 the relevant mathematical foundations, which include the basics of compressive sensing, block sparse solver, basics of frames and Khatri-Rao product. In Section 3, we discuss the basics of tomography and its discrete formulation. In Sections 4 and 5, we present the motivation for current work and the proposed algorithm for LVCT, respectively. In the last 3 Sections, we discuss the simulation results, some concluding remarks and the proof of a result involving Khatri-Rao product, respectively.

2 Relevant mathematical foundations

This section introduces the essential mathematical foundations such as compressive sensing, the notion of block sparsity, the Total Variation Augmented Lagrangin and aLternating direction aLgorithm (TVAL3), equi-angular tight frames and the Khatri-Rao product that are relevant to the objectives of the present work. In the subsequent part of the paper, the concept of block sparsity, equi-angular tight frames and Khatri-Rao product, for instance, are used for identifying the optimal set of views for LVCT. The TVAL3 algorithm, on the other hand, is used for reconstructing the CT images from the optimal set of projection-views so determined.

2.1 Compressive sensing

Compressive sensing (CS) is a mathematical technique capable of reconstructing a sparse signal (or signal that is compressible or sparse in some domain) from a few of its linear measurements [33]. Define $\|x\|_0 := |\{j : x_j \neq 0\}|$, the number of non-zero coefficients in vector x. For $A \in \mathbb{R}^{m\times n}$ ($m << n$), suppose $y = Ax + e$ is a measurement vector where $e \in \mathbb{R}^m$ is a noise vector with $\|e\|_2 \leq \varepsilon$, with ε standing for the noise power. One may pose the sparse signal recovery problem as the following minimization problem [7, 28, 33, 39]:

$$(P_0) \quad \min_{x\in\mathbb{R}^n} \|x\|_0 \quad subject \quad to \quad \|y - Ax\|_2 \leq \varepsilon. \tag{1}$$

Since the P_0 minimization problem becomes NP-hard [33] as the dimension increases, the convex relaxation of P_0 problem is proposed [3, 11] as

$$(P_1) \quad \min_{x\in\mathbb{R}^n} \|x\|_1 \quad subject \quad to \quad \|y - Ax\|_2 \leq \varepsilon. \tag{2}$$

The mutual coherence $\mu(A)$ of a matrix A is the largest absolute normalized inner-product between different columns of it, that is,

$$\mu(A) = \max_{1\leq i,j\leq n, i\neq j} \frac{|< a_i, a_j >|}{\|a_i\|_2 \|a_j\|_2}, \tag{3}$$

where a_i denotes the i^{th} column of A. The total coherence [38] of a matrix $\mu_t(A)$ is defined as follows:

$$\mu_t(A) = \left(\sum_{i\neq j, 1\leq i,j\leq n} \left(\frac{|\langle a_i, a_j \rangle|}{\|a_i\|_2 \|a_j\|_2} \right)^2 \right)^{1/2}, \tag{4}$$

The following relation holds [1] true for a matrix A of size $m \times n$:

$$\mu_W := \sqrt{\frac{n-m}{m(n-1)}} \leq \mu(A) \leq \mu_t(A), \tag{5}$$

where μ_W is the lower bound for $\mu(A)$ and is also known as the Welch bound. Smaller values for $\mu(A)$ and $\mu_t(A)$ imply better sparse recovery guarantees [29, 38].

2.2 TVAL3

In [15, 19], the authors have studied the total variation augmented Lagrangian and alternating direction algorithm (TVAL3) for the TV-regularized CS problems. It has become popular due to its efficiency and high tolerance. The TVAL3 algorithm has shown promising results in CT applications [24]. For a sparsifying transform W, let v denote Wx, then one obtains the total variation model to solve $z = Ax$ for its sparse solution via

$$\mathscr{P}_{tv1} : \min_{v,x} \|v\|_1 \text{ subject to } Ax = z,\ v = Wx. \tag{6}$$

The corresponding augmented Lagrangian function of this minimization problem is

$$\mathscr{P}_{al}: \min_{v,x} \Big[\|v\|_1 - \beta_1^T (Wx - v) + \frac{\beta_2}{2}\|Wx - v\|_2^2 - \beta_3^T (Ax - z) + \frac{\beta_4}{2}\|Ax - z\|_2^2 \Big]. \tag{7}$$

which is solved by the alternating direction method. In applications, popular sparsifying transforms are provided by the gradient operator, wavelets etc. A detailed description of TVAL3 along with the selection of β_i, $i = 1,2,3,4$ can be seen in [15–17] and the references therein.

2.3 Block sparsity

In many practical applications, such as recovery of multi-band signals [20], measurements of gene expression levels [23] and the identification of online smart grid topology [2], the signals are block-sparse, that is, the non-zero components of a vector x lie in the form of blocks. To define block sparsity [5, 18, 37], one considers x as a concatenation of blocks of length s with $x[l]$ as the l^{th} block, that is,

$$x = [\underbrace{x_1 \dots x_s}_{x^T[1]} \quad \underbrace{x_{s+1} \dots x_{2s}}_{x^T[2]} \quad \dots \quad \underbrace{x_{n-s+1} \dots x_n}_{x^T[L]}]^T, \tag{8}$$

where $n = Ls$. A vector x is called block $K-$sparse if $x[l]$ has a nonzero euclidean norm for K number of indices l. That is, $\|x\|_{2,0} = K$, where

$$\|x\|_{2,0} = \sum_{l=1}^{L} I(\|x[l]\|_2 > 0) \tag{9}$$

with I being the indicator function satisfying $I(\|x[l]\|_2 > 0) = \begin{cases} 1 \text{ if } \|x[l]\|_2 > 0, \\ 0 \text{ otherwise.} \end{cases}$

When $s = 1$, the notion of block sparsity coincides with the standard sparsity. The matrix A can also be denoted in the same way as follows:

$$A = [\underbrace{a_1 \dots a_s}_{A^T[1]} \quad \underbrace{a_{s+1} \dots a_{2s}}_{A^T[2]} \quad \dots \quad \underbrace{a_{n-s+1} \dots a_n}_{A^T[L]}]^T. \tag{10}$$

The most widely used recovery algorithm for block sparse vectors is based on the classical orthogonal matching pursuit (OMP) [36], and it is referred to as block orthogonal matching pursuit (BOMP) [5, 18, 37]. The non-negative BOMP [18] finds the non-negative block sparse approximation of an underdetermined matrix equation.

The performance guarantee of BOMP depends on the block-coherence (μ_B) and block sub-coherence (ν_B) of normalized matrix A which are defined as follows [5]:

$$\mu_B = \frac{1}{s} \max_{l \neq r} \sqrt{\lambda_{max}\big(M[l,r]\big)},$$

where $M[l,r] = A^T[l]A[r]$ and $\lambda_{max}\big(M[l,r]\big)$ denotes the maximum eigen value of $(M[l,r])$. The block sub-coherence is defined as:

$$\nu_B = \max_{l} \max_{i \neq j} |\langle a_i, a_j \rangle|, \quad \forall a_i, a_j \in A[l].$$

The recovery guarantees of the block solvers via block-coherence are less-pessimistic compared to that of OMP through the classical coherence [5].

2.4 Equiangular tight frames

We introduce the notion of frames [4] briefly as this concept is used in a later section. For $n \geq m$, a sequence of vectors $\{h_l\}_{l=1}^n$ is called a frame for $\mathbb{C}^m$, if there exist $0 < \alpha \leq \beta < \infty$ such that

$$\alpha \|x\|_2^2 \leq \sum_{l=1}^{n} |\langle x, h_l \rangle|^2 \leq \beta \|x\|_2^2, \quad \forall x \in \mathbb{C}^m, \tag{11}$$

where α and β are called the frame bounds. If $\alpha = \beta$, $\{h_l\}_{l=1}^n$ is called a tight frame. We now define an equiangular tight frame.

Definition 1 A tight frame $\{h_l\}_{l=1}^n$ is called an equiangular tight frame (ETF) [6], if it satisfies the following properties:

1. $\|h_l\|_2 = 1, \forall l,$
2. $|\langle h_i, h_l \rangle| = \gamma, \forall i \neq l.$

If H is a Gram matrix of an ETF (that is, the $(i,j)^{th}$ element of H is $\langle h_i, h_j \rangle$), then the off-diagonal entries of H have the same magnitude as γ. Ideally, the Gram matrix of an ETF is expected to belong to the convex set:

$$\mathscr{H}_{\mu_W} = \{H \in \mathbb{R}^{n \times n} : H = H^T,\ H_{ii} = 1,\ max_{i \neq j} |H_{ij}| \leq \mu_W\}, \tag{12}$$

where μ_W is defined in (5). If $\tilde{H}$ is the Gram matrix of an initial sensing matrix, the matrix H, whose elements are defined the following way [30], falls in $\mathscr{H}_{\mu_W}$.

$$H_{i,j} = \begin{cases} 1, & i = j, \\ \tilde{H}_{i,j}, & i \neq j, |H_{i,j}| \leq \mu_W, \\ sign(\tilde{H}_{i,j})\mu_W, & else. \end{cases} \tag{13}$$

In this work, we make use of the afore-stated projection strategy in determining an optimal set of measurements for LVCT, which is discussed in Section 5.

2.5 Khatri-Rao product

Suppose $\tilde{P} = [\tilde{p}_{i,j}]$ and $\tilde{Q} = [\tilde{q}_{i,j}]$ are two matrices of sizes $\tilde{m} \times \tilde{n}$ and $\tilde{l} \times \tilde{n}$ respectively, and $\tilde{p}_i$ and $\tilde{q}_j$ denote the i^{th} and j^{th} columns of these matrices $\tilde{P}$ and $\tilde{Q}$ respectively, then the Khatri-Rao product [27] is obtained as follows:

$$\tilde{P} \odot \tilde{Q} = [\tilde{p}_1 \otimes \tilde{q}_1 \quad \tilde{p}_2 \otimes \tilde{q}_2 \quad \dots \quad \tilde{p}_{\tilde{n}} \otimes \tilde{q}_{\tilde{n}}]. \tag{14}$$

In (14), the symbol $\otimes$ denotes the Kronecker product satisfying

$$\tilde{p}_i \otimes \tilde{q}_i = [\tilde{p}_{1,i}\, \tilde{q}_i^T \ \dots \ \tilde{p}_{\tilde{m},i}^T\, \tilde{q}_i]^T, \ \text{for } i = 1,2\dots\tilde{n}. \tag{15}$$

Hence the resultant matrix $\tilde{P} \odot \tilde{Q}$ is of size $\tilde{m}\tilde{l} \times \tilde{n}$ with i^{th} column being $\tilde{p}_i \otimes \tilde{q}_i$. Suppose vec$(X)$ is a vectorization operation performed on X. For example, for a matrix X of size $\tilde{n} \times \tilde{l}$, vec$(X)$ is an $\tilde{n}\tilde{l} \times 1$ column vector, which is obtained by stacking the columns of the matrix one below the other in order.

When X is a diagonal matrix of size $\tilde{n} \times \tilde{n}$, and $\tilde{P}$ and $\tilde{Q}$ are of sizes $\tilde{m} \times \tilde{n}$ and $\tilde{n} \times \tilde{q}$ respectively, the following relation holds:

$$\text{vec}(\tilde{P}X\tilde{Q}) = (\tilde{Q}^T \odot \tilde{P})\, \text{Diag}(X). \tag{16}$$

In (16), $Diag(X)$ is considered as a column vector with diagonal elements of X as its elements. The proof of above relation is provided in Section 10, which is provided as an appendix.

3 Computed tomography and its discrete formulation

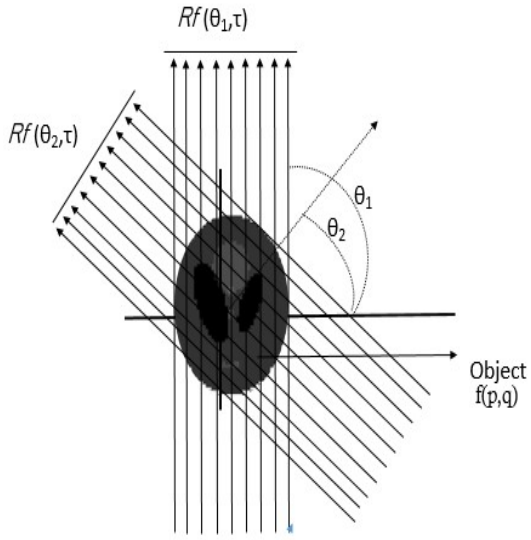
For any angular parameter $\theta \in [0,\pi)$ and radial parameter $\tau \in (-\infty,\infty)$, the Radon transform [13] of a sufficiently nice function f is defined as

$$(Rf)(\theta,\tau) = \int_{-\infty}^{\infty}\int_{-\infty}^{\infty} f(p,q)\delta(p\cos\theta + q\sin\theta - \tau)\,dp\,dq, \tag{17}$$

which is referred to as a projection or Radon measurement corresponding to the radial and angular pair (τ,θ). The Radon transform in (17) determines the total density of a function f along the line $p\cos\theta + q\sin\theta = \tau$. This line is defined by an angle θ from the p-axis and a distance r from the origin. Beer's law illustrates the relationship between the measured intensity data and the Radon transform as follows:

$$log\left(\frac{I_{source}}{I_{detector}}\right) = (Rf)(\theta,r).$$

Here, I_{source} and $I_{detector}$ represent the intensities at the X-ray source and detector, respectively. Since I_{source} and



(a)

Fig. 1: Data collection in CT for different radial and angular parameters.

$I_{detector}$ can be measured, the Radon transform Rf in equation (17) is known. The filter back-projection [13] is a popular method for reconstructing f from the known projection data $\{(Rf)(\theta,\tau) : \theta \in [0,\pi),\ \tau \in (-\infty,\infty)\}$.

In discrete setting, however, f is a two dimensional (2D) image such that $f \in \mathbb{R}^{M\times M}$. With $\delta\tau$ acting as the increment in radial sampling, the discretization of angular (θ) and radial (τ) parameters in parallel beam geometry (shown in Figures 1 and 2) is achieved by

$$\tau_j = \delta\tau\left(j - \frac{M}{2}\right),\ \theta_i = \frac{i+0.5}{M}\pi, \text{ for } i,j \in \{0,1,\cdots,M-1\}, \tag{18}$$

where M^2 is the number of pixels in the image. Thus the discrete form of (17) is as follows:

$$(Rf)(\theta_i,\tau_j) = \sum_l \Phi_{i,j}(l)x_l, \tag{19}$$

where $x \in \mathbb{R}^n$ is the vector form of $f \in \mathbb{R}^{M\times M}$ with $n = M^2$ and

$$\Phi_{i,j}(l) = \begin{cases} w_{ij} & \text{if } (\theta_i,\tau_j) \text{ hits } l^{th} \text{ pixel, for } l = 1,2\dots,M, \\ 0 & \text{else,} \end{cases}$$

where $w_{i,j}$ is the weight of the ray, that is governed by θ_i and τ_j, in each pixel. It may be noted that x_l denotes the intensity

value of the underlying image at l^{th} pixel. The equation (19) may be rewritten as

$$(Rf)(\theta_i,\tau_j) = [\Phi_{i,j}(1)\dots\Phi_{i,j}(n)][x_1\dots x_n]^T. \tag{20}$$

From all θ_i and τ_j, one generates a matrix system

$$y = \Phi x. \tag{21}$$

Many efficient algorithms have been proposed to recover the underlying image (x) from the Radon measurements (y) [9, 15]. The vector $y \in \mathbb{R}^{n\times 1}$ and the matrix $\Phi \in \mathbb{R}^{n\times n}$ may be viewed to have a block structure as stated below:

$$y = \begin{bmatrix} [(Rf)(\theta_0,\tau_j)]_{j=0}^{M-1} \\ [(Rf)(\theta_1,\tau_j)]_{j=0}^{M-1} \\ \vdots \\ [(Rf)(\theta_{M-1},\tau_j)]_{j=0}^{M-1} \end{bmatrix}, \quad \Phi = \begin{bmatrix} [(\Phi)(\theta_0,\tau_j)]_{j=0}^{M-1} \\ [(\Phi)(\theta_1,\tau_j)]_{j=0}^{M-1} \\ \vdots \\ [(\Phi)(\theta_{M-1},\tau_j)]_{j=0}^{M-1} \end{bmatrix}. \tag{22}$$

From here on, we denote the k^{th} $M\times n$ angular block of Φ as $\Phi_k = [(\Phi)(\theta_k,\tau_j)]_{j=0}^{M-1}$, which refers to $[\Phi_{i,j}(l)]$ for each fixed i in (19).

As X-rays are very harmful to human bodies, any reduction in the quantity of X-ray dosage to be given in CT is extremely beneficial. In LVCT, however, X-ray dosage is taken corresponding to a few angles. That is, a set of blocks is used. Consequently, LVCT reduces the X-ray dosage by avoiding using some of the angular blocks.

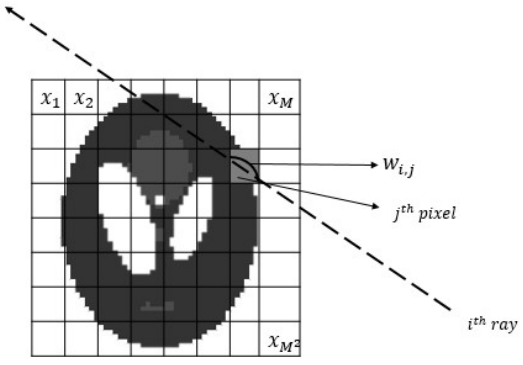


Fig. 2: Discretization of Radon transform

4 Motivation for present work

For the purpose of demonstrating significance of the optimal angles we show in Table 1 the reconstructions obtained with different sets of 13 views by setting M to 32 in (18). The reconstructions via TVAL3 solver with these different sets of limited-view data are reported in Figure 3 with PSNR measures (defined in Section 6) and in Table 1, which show that the choice of angular blocks has a bearing on the reconstruction quality. In general, in LVCT, views are taken over some limited angular parameters. If we are given the number of views (say K) in advance, then we generally do not know which set of K views is optimal (or preferable) in image reconstruction. To the best of our knowledge, existing results, as discussed in Section 1, do not determine an optimal set of views that are good enough for reconstrction of reliable quality. Motivated by this gap in the literature, in this paper, we propose a sparsity based optimization strategy for finding an angular set of views that are optimal for CS based CT image reconstruction.

Table 1: For the five sets of views (shown in the second column) where the angular parameters lie in $\left\{\theta_i = \frac{i+0.5}{32}\pi, \text{ for } i \in \{0,1,\cdots,31\}\right\}$, where the reconstructions are obtained by solving (21). This table, stating the reconstruction qualities in PSNR terms, justifies that the fifth set (arising out of proposed method, which is discussed in Section 5) provides superior reconstruction quality.

Set	Projection angles θ_i considered where i takes values	PSNR
1	$1,2,3\dots12,13$	18.5437
2	$14,15,16\dots25,26$	20.0912
3	as provided by the random sampling	24.1086
4	$1,3,5\dots23,25$	27.6758
5	as provided by a deterministic sampling strategy (Proposed)	37.1655

5 Proposed block-sparse method

In this section, we present our deterministic angular sampling strategy for LVCT in such a way that the corresponding sub-Radon matrix has good sparse recovery properties. In view of the ETFs having good conditioning and low coherence, if we can select the angular parameters in such a way that the corresponding sub-Radon matrix is close to an ETF, then it admits good sparse recovery properties.

It may be observed that removal or de-selection of the k^{th} view from the Radon matrix Φ (discussed in Section 3) means deletion of the k^{th} $M\times n$ angular block $\Phi_k = [(\Phi)(\theta_k,\tau_j)]_{j=0}^{M-1}$ from Φ. Consequently, we can view the angle-selection as the selection of angular blocks from the Radon matrix. This step in turn can be viewed as a preconditioning technique where the square preconditioner is a diagonal matrix (whose diagonal vector is a block sparse vector)

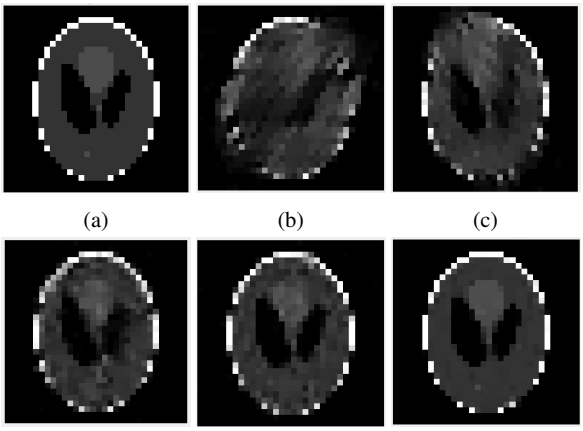


Fig. 3: For the test image in (a), the images in (b) to (f) correspond to reconstruction with different sets of 13 views that are from set 1 to set 5 as shown in Table 1. In (a), original phantom is shown. This figure along with the PSNR-measures shown in Table implies that the sub-sampling strategy impacts reconstruction quality.

and views correspond to the non-zero blocks, which are precisely the selected ones. Therefore, the problem of selecting $K(< M)$ optimal views is equivalent to finding a diagonal matrix with $K-$block sparse diagonal vector so that the resulting preconditioned sub-Radon matrix is close to an ETF. We discuss in what follows the formulation of block sparse model in detail.

Let us consider the Radon matrix $\Phi_{n\times n}$ that is defined in Section 3. We now find the row-restricted block Radon matrix $\Psi_{(KM\times n)}$ of Φ such that Ψ is close to an ETF. The K row block selection can be done by pre-multiplying Φ by a diagonal matrix $D_{n\times n}$ whose diagonal vector d (that is, $d = Diag(D)$) is a $K-$block sparse vector where each block is of size M. At the end we obtain Ψ after removing $(M-K)M$ zero rows from $D\Phi$, where $D\Phi$ has the following form:

$$D\Phi = \begin{bmatrix} (d_0)_{M\times 1} & & \\ & \ddots & \\ & & (d_{M-1})_{M\times 1} \end{bmatrix} \begin{bmatrix} [(\Phi)(\theta_0,\tau_j)]_{j=0}^{M-1} \\ \vdots \\ \vdots \\ [(\Phi)(\theta_{M-1},\tau_j)]_{j=0}^{M-1} \end{bmatrix}. \tag{23}$$

The block sparsity $\|d\|_{2,0}$ of the diagonal vector $d = [d_0\, d_1 \cdots d_{M-1}]$ is K, that is, K blocks are non-zero. Therefore, in order to find an optimal Ψ_{Opt}, we find an optimal D_{Opt} such that the Gram matrix $(D_{Opt}\Phi)^T(D_{Opt}\Phi)$ is close to H, where H is the Gram matrix of an ETF as constructed in Section 2.4, that is,

$$\Phi^T D_{Opt}^2 \Phi \approx H. \tag{24}$$

In view of above approximation, we have $\text{vec}(\Phi^T D_{Opt}^2 \Phi) \approx \text{vec}(H)$, which implies

$$(\Phi^T \odot \Phi^T)\text{Diag}(D_{Opt}^2) \approx \text{vec}(H), \tag{25}$$

where $Diag(D_{Opt}^2)$ is a vector of size n. The equation (25) can be equivalently posed as the following non-negative block sparse recovery problem

$$d_{Opt} = \arg \min_{d\geq 0, \|d\|_{2,0}\leq K} \|(\Phi^T \odot \Phi^T)d - \text{vec}(H)\|_2. \tag{26}$$

The afore-formulated block sparse optimization problem can be solved by the existing non-negative BOMP algorithm [18] for an optimal $K-$block sparse vector d_{Opt}. Finally, the optimal mask D_{Opt} is determined such that $d_{Opt} = Diag(D_{Opt}^2)$ holds. Now, the indices of the K non-zero blocks of the diagonal matrix D_{Opt} are precisely the K optimal views.

Remark 1 It is to be noted that the present reconstruction of LVCT needs sparsity-driven methods at 2 stages. The first stage involves finding the optimal subset of views via block-diagonal pre-conditioning, which is precisely the contribution of the present work. The second stage involves solving the sub-sampled system (an undermined matrix equation)

$$D_{Opt}y = D_{Opt}\Phi x \tag{27}$$

for its sparse solution. In (27), D_{Opt} is obtained via (26), where the pair (y,Φ) is stated as in (21). This step can be executed using any popular sparse signal recovery solver [15]. The overall execution strategy of the proposed LVCT is summarized in Algorithm 1.

6 Numerical results

In this section, we show that the sparse recovery properties of the sensing matrix obtained via the methodology proposed in Section 5 are better than their counterparts that involve random sub-sampling. Consequently, the proposed method is supposed to produce a reconstruction of superior quality. In general, as quality in reconstruction problems is ascertained through the standard metrics like PSNR, MSE and SSIM, we use them in our simulation work. The PSNR value is computed as

$$PSNR = 10log_{10}\frac{\|x_r\|_\infty^2}{\|x-x_r\|_2}. \tag{28}$$

Algorithm 1: LVCT Algorithm

- **Input:**
  (1). Discrete Radon matrix $\Phi_{n\times n}$, where n is the number of image-pixels.
  (2). K (number of angular blocks)
- **Finding optimal views**
  (1). Obtain the block sparse vector d_{Opt} from

$$\min_{d\geq 0, \|d\|_{2,0}\leq K} \|(\Phi^T \odot \Phi^T)d - \mathrm{vec}(H)\|_2.$$

  (2). Optimal mask D_{Opt} is determined from $d_{Opt} = Diag(D^2_{Opt})$.
- **Reconstructing image from the limited views**
  Obtain x from

$$\min_{v,x} \left[\|v\|_1 - \beta_1^T \eta_1 + \frac{\beta_2}{2}\|\eta_1\|_2^2 - \beta_3^T \eta_2 + \frac{\beta_4}{2}\|\eta_2\|_2^2 \right],$$

  where, $\eta_1 = \nabla x - v$ and $\eta_2 = D_{Opt}\Phi x - D_{Opt} y$, with *gradient* as sparsifying transform in (7).
- **Output:**
  Reconstructed image x.

The relative reconstruction error is computed as

$$MSE = \frac{\|x - x_r\|_2}{\|x\|_2}. \tag{29}$$

In (28) and (29), x and x_r are the original and recovered images (in vector form) respectively.

The structural similarity (SSIM) index [35] is a widely used metric for assessing the structural similarity between two images x and x_r. To compare these images, consider ρ and t as local patches extracted from both the images. The SSIM index evaluates three key aspects of similarity between these patches: (i) luminance similarity $l(\rho,t)$, (ii) contrast similarity $c(\rho,t)$, and (iii) structural similarity $s(\rho,t)$. The local SSIM value is then computed as follows:

$$\begin{aligned} S(\rho,t) &= l(\rho,t)\cdot c(\rho,t)\cdot s(\rho,t) \\ &= \left(\frac{2\mu_\rho\mu_t + C_1}{\mu_\rho^2 + \mu_t^2 + C_1}\right)\left(\frac{2\sigma_\rho\sigma_t + C_2}{\sigma_\rho^2 + \sigma_t^2 + C_2}\right)\left(\frac{2\sigma_{\rho t} + C_3}{\sigma_\rho\sigma_t + C_3}\right). \end{aligned} \tag{30}$$

In this equation, μ_ρ and μ_t represent the local means, σ_ρ and σ_t are local standard deviations, and $\sigma_{\rho t}$ denotes cross-correlation after removing their means. The constants C_1, C_2 and C_3 serve as stabilizers. One computes the SSIM index of entire image by pooling the SSIM map (that is, by simply averaging the SSIM map). The SSIM index is recognized for its effectiveness in evaluating image quality, with higher SSIM values indicating better reconstruction quality [35].

Suppose K signifies the number of required blocks that represent the views in our selection. Our aim is to select a Radon matrix of size $KM \times n$ possessing lower total coherence, which is a concatenation of these K blocks. The stated objective is realized by using the methodology discussed in Section 5. We demonstrate the simulation work using a Shepp-Logan phantom image [21] of resolution 32×32. For the sake of convenience, we set each of number of angular parameters and number of radial parameters to 32. Hence the corresponding full Radon matrix is concatenation of 32 blocks, each of size 32×1024. As the random matrices (whose entries are independent and identically distributed Gaussian random variables) possess optimal recovery guarantees [30], we envisage that the H in (26), that is the projection of the Gram matrix of the random matrix, is an optimal choice.

We have obtanied D_{Opt} by solving (26). We have then computed the total coherences of $D_{Opt}\Phi$ and $D_{Rand}\Phi$ where $D_{Rand}\Phi$ picks the K blocks of Φ via uniform distributions. Table 2 compares the total coherences of $D_{Rand}\Phi$ and $D_{Opt}\Phi$. This table demonstrates that the total coherence of the $D_{Opt}\Phi$ is smaller, indicating that it provides better reconstruction. In terms of PSNR, SSIM, and relative l_2 error, Table 3 demonstrates how well the images are reconstructed, which shows that the proposed deterministic-LVCT provides better recovery outcomes than the random-LVCT for all under sampled data, The results in Tables 2 and 3 are in agreement with the fact that the proposed method optimizes the sub-sampling procedure. Using TVAL3 algorithm, we have reconstructed the images from $D_{Rand}\, y = D_{Rand}\Phi x$ and $D_{Opt}\, y = D_{Opt} x$ for different values of K. The results shown in Figure 4 conform to the improved total coherences.

Table 2: For K number of views (where $K = 13, 15, 17, 19, 21, 23$), the total coherences $\mu_t(D_{Opt}\Phi)$ and $\mu_t(D_{Rand}\Phi)$ of deterministically and randomly sub-sampled Radon matrix are shown in this table. This table implies smaller total coherence for $D_{Opt}\Phi$, which implies relatively better behaviour in sparse signal recovery.

K	$\mu_t(D_{Rand}\Phi)$	$\mu_t(D_{Opt}\Phi)$
13	58.9356	55.4589
15	58.0986	55.2675
17	57.4198	54.8854
19	56.6845	55.2595
21	54.5789	53.4598
23	53.8734	52.1935

7 Conclusion

In this paper, with a view to obtaining a reconstruction of better quality, we have presented a deterministic angular sampling strategy for LVCT, as an alternative to existing random sampling. For obtaining the optimal angular sampling,

Table 3: For the test image shown in Figure 3(a) and for K views (K = 13, 15, 17, 19, 21, 23, 25), this table provides the reconstruction qualities (through PSNR, SSIM and relative l_2 error measures) of the randomly and deterministically sub-sampled LVCT. These results show the reconstruction of better quality via the proposed deterministic strategy.

K	Random-LVCT			Deterministic-LVCT		
	PSNR	SSIM	Error l_2	PSNR	SSIM	Error l_2
13	26.5746	0.9589	0.1654	37.1655	0.9953	0.0437
15	28.5503	0.9679	0.1283	37.1291	0.9938	0.0453
17	31.2892	0.9801	0.1022	39.0578	0.9970	0.0349
19	33.2217	0.9870	0.0837	41.4383	0.9979	0.0271
21	35.1093	0.9898	0.0658	41.9138	0.9981	0.0269
23	37.5218	0.9946	0.0534	42.2011	0.9985	0.0270

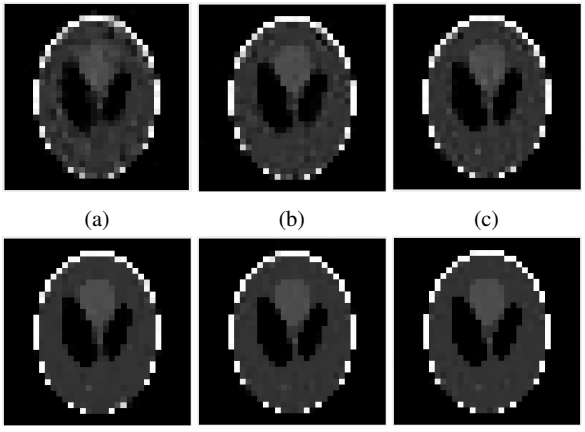


Fig. 4: For 13, 17, and 19 views, this figure provides the reconstructions with random-LVCT in (a), (b) and (c), and with the proposed deterministic-LVCT in (d) (e), and (f). The test image considered is shown in Figure 3(a). This figure demonstrates the improvement in performance by the proposed deterministic LVCT.

we have used techniques from compressive sensing involving non-negative block sparse recovery. We have demonstrated its efficacy through simulation work and compare it with its random counterpart.

The optimal solution d_{Opt} provided by (26) is typically dependent on the choice of H. Optimizing the problem in (26) also with respect to $H \in \mathscr{H}_{\mu_W}$, as defined in (12), is very challenging. Our future efforts will attempt to address this problem.

8 Conclusion

In this paper, we have presented a deterministic angular sampling strategy for LVCT, as an alternative to existing random sampling, in order to obtain a reconstruction of better quality. For otbaiting optimal angular sampling, we have used techniques from compressed sensing involving non-negative block sparse recovery. We have demonstrated its efficacy through simulation work while comparing it with its random counterpart.

9 Declarations

Availability of supporting data: Not Applicable.
Competing interests: The authors declare that they have no conflict of interest.
Funding: The authors received support and fund from CSIR (No. 25(0309)/20/EMR-II) India during the preparation of this manuscript.
Ethical approval: Not Applicable.
Authors' contributions: All the authors contributed equally to the manuscript and went through it completely.
Acknowledgments The first and the third authors gratefully acknowledge the support received from the CSIR (No. 25(0309)/20/EMR-II) India.

References

1. V. Abolghasemi, S. Ferdowsi, and S. Sanei. A gradient-based alternating minimization approach for optimization of the measurement matrix in compressive sensing. *Signal Processing*, 92(4):999–1009, 2012.
2. M. Babakmehr, M. G. Simões, M. B. Wakin, and F. Harirchi. Compressive sensing-based topology identification for smart grids. *IEEE Transactions on Industrial Informatics*, 12(2):532–543, 2016.
3. E. J. Candes. The restricted isometry property and its implications for compressed sensing. *Comptes rendus mathematique*, 346(9-10):589–592, 2008.
4. O. Christensen et al. *An introduction to frames and Riesz bases*, volume 7. Springer, 2003.
5. Y. C. Eldar, P. Kuppinger, and H. Bolcskei. Block-sparse signals: Uncertainty relations and efficient recovery. *IEEE Transactions on Signal Processing*, 58(6):3042–3054, 2010.
6. D. Goyeneche and O. Turek. Equiangular tight frames and unistochastic matrices. *Journal of Physics A: Mathematical and Theoretical*, 50(24):245304, 2017.
7. F. Gu and A. Wan. Nonconvex p-α q minimization method and p-rip condition for stable recovery of approximately k-sparse signals. *Computational and Applied Mathematics*, 43(1):29, 2024.
8. Y. Gui, X. Zhao, Y. Bai, R. Zhao, W. Li, and Y. Liu. Low-dose ct iterative reconstruction based on image block classification and dictionary learning. *Signal, Image and Video Processing*, 17(2):407–415, 2023.
9. P. C. Hansen and J. S. Jørgensen. Air tools II: algebraic iterative reconstruction methods, improved implementation. *Numerical Algorithms*, 79(1):107–137, 2018.
10. M. S. Islam and R. Islam. Generalized gaussian model-based reconstruction method of computed tomography image from fewer projections. *Signal, Image and Video Processing*, 14(3):547–555, 2020.

11. C. Kennedy and R. Ward. Greedy variance estimation for the lasso. *Applied Mathematics & Optimization*, 82(3):1161–1182, 2020.
12. S. Kirkpatrick, C. D. Gelatt Jr, and M. P. Vecchi. Optimization by simulated annealing. *science*, 220(4598):671–680, 1983.
13. P. Kuchment. *The Radon transform and medical imaging*. SIAM, 2013.
14. N.-Y. Lee and B. J. Lucier. Wavelet methods for inverting the radon transform with noisy data. *IEEE transactions on image processing*, 10(1):79–94, 2001.
15. C. Li. *An efficient algorithm for total variation regularization with applications to the single pixel camera and compressive sensing*. Rice University, 2010.
16. C. Li, W. Yin, H. Jiang, and Y. Zhang. Improved total variation-based ct image reconstruction applied to clinical data. *Physics in Medicine and Biology*, 56(6):1545 – 1561, 2011.
17. C. Li, W. Yin, H. Jiang, and Y. Zhang. An efficient augmented lagrangian method with applications to total variation minimization. *Computational Optimization and Applications*, 56(3):507–530, 2013.
18. H. Li and Q. Chen. Analysis of non-negative block orthogonal matching pursuit. *Wireless Personal Communications*, pages 1–14, 2022.
19. Z. Liu, H. Liu, and X. Wang. Accelerated augmented lagrangian method for total variation minimization. *Computational and Applied Mathematics*, 38:1–15, 2019.
20. M. Mishali and Y. C. Eldar. Blind multiband signal reconstruction: Compressed sensing for analog signals. *IEEE Transactions on signal processing*, 57(3):993–1009, 2009.
21. J. L. Mueller and S. Siltanen. *Linear and nonlinear inverse problems with practical applications*. SIAM, 2012.
22. A. Nagy and A. Kuba. Reconstruction of binary matrices from fan-beam projections. *Acta Cybernetica*, 17(2):359–383, 2005.
23. F. Parvaresh, H. Vikalo, S. Misra, and B. Hassibi. Recovering sparse signals using sparse measurement matrices in compressed dna microarrays. *IEEE Journal of Selected Topics in Signal Processing*, 2(3):275–285, 2008.
24. L. Ritschl, F. Bergner, C. Fleischmann, and M. Kachelrieß. Improved total variation-based ct image reconstruction applied to clinical data. *Physics in Medicine & Biology*, 56(6):1545, 2011.
25. T. Schüle, C. Schnörr, S. Weber, and J. Hornegger. Discrete tomography by convex–concave regularization and dc programming. *Discrete Applied Mathematics*, 151(1-3):229–243, 2005.
26. M. Sonkar, P. Sasmal, P. Theeda, and C. Sastry. Sparsity-driven deterministic sampling strategy for coded aperture X-ray computed tomography. *Measurement Science and Technology*, 33(3):034003, 2021.
27. M. Sørensen and L. De Lathauwer. Multidimensional harmonic retrieval via coupled canonical polyadic decomposition—part i: Model and identifiability. *IEEE Transactions on Signal Processing*, 65(2):517–527, 2016.
28. P. J. Tardivel, R. Servien, and D. Concordet. Sparsest representations and approximations of an underdetermined linear system. *Inverse Problems*, 34(5):055002, 2018.
29. P. Theeda, P. P. Kumar, C. S. Sastry, and P. V. Jampana. Reconstruction of sparse-view tomography via preconditioned radon sensing matrix. *Journal of Applied Mathematics and Computing*, 59(1):285–303, 2019.
30. E. Tsiligianni, L. P. Kondi, and A. K. Katsaggelos. Preconditioning for underdetermined linear systems with sparse solutions. *IEEE Signal Processing Letters*, 22(9):1239–1243, 2015.
31. L. Varga, P. Balázs, and A. Nagy. Direction-dependency of a binary tomographic reconstruction algorithm. In *Computational Modeling of Objects Represented in Images: Second International Symposium, CompIMAGE 2010, Buffalo, NY, USA, May 5-7, 2010. Proceedings 2*, pages 242–253. Springer, 2010.
32. L. Varga, P. Balázs, and A. Nagy. Projection selection algorithms for discrete tomography. In *Advanced Concepts for Intelligent Vision Systems: 12th International Conference, ACIVS 2010, Sydney, Australia, December 13-16, 2010, Proceedings, Part I 12*, pages 390–401. Springer, 2010.
33. M. Vidyasagar. *An introduction to compressed sensing*. SIAM, 2019.
34. C. Wang, Y. He, K. Zhao, and W. Yu. A fast regularized ct reconstruction method based on a preconditioning matrix for limited-angle fan-beam ct. *Applied Mathematics Letters*, 150:108950, 2024.
35. Z. Wang, A. C. Bovik, H. R. Sheikh, and E. P. Simoncelli. Image quality assessment: from error visibility to structural similarity. *IEEE transactions on image processing*, 13(4):600–612, 2004.
36. J. Wen and H. Li. Binary sparse signal recovery with binary matching pursuit. *Inverse Problems*, 37(6):065014, 2021.
37. C. Xia, Y. Gao, J. Yu, and Z. Yu. Block-sparse signal recovery based on orthogonal matching pursuit via stage-wise weak selection. *Signal, Image and Video Processing*, 14(1):97–105, 2020.
38. R. Yi, C. Cui, B. Wu, and Y. Gong. A new method of measurement matrix optimization for compressed sensing based on alternating minimization. *Mathematics*, 9(4):329, 2021.
39. Z. Zhu, J. Ma, and B. Zhang. A new conjugate gradient hard thresholding pursuit algorithm for sparse signal recovery. *Computational and Applied Mathematics*, 39:1–20, 2020.

10 Appendix

Lemma 1 *Suppose X is a diagonal matrix of size $\tilde{n}\times\tilde{n}$, and the matrices $\tilde{P}$ and $\tilde{Q}$ are of sizes $\tilde{m}\times\tilde{n}$ and $\tilde{n}\times\tilde{q}$ respectively. Then the following relation holds:*

$$vec(\tilde{P}X\tilde{Q}) = (\tilde{Q}^T \otimes \tilde{P})vec(X) = (\tilde{Q}^T \odot \tilde{P})Diag(X),$$

where $Diag(X)$ is the vector whose elements are the diagonal components of X.

Proof Suppose the diagonal elements of X are $x_1, x_2, \ldots x_{\tilde{n}}$. $\tilde{P} = [\tilde{p}_{i,j}]$ and $\tilde{Q} = [\tilde{q}_{i,j}]$. Then it is easy to show that

$$(\tilde{P}X\tilde{Q})_{i,j} = \sum_{l=1}^{\tilde{n}} \tilde{p}_{i,l}\, x_l\, \tilde{q}_{l,j}.$$

As $vec(X)$ has nonzero entries at designated places, from the definition of Kronecker product, it follows that

$$(\tilde{Q}^T \otimes \tilde{P})\mathrm{vec}(X) = \sum_{i=1}^{\tilde{n}} x_i\, (\tilde{q}_i^T \otimes \tilde{p}_i),$$

where $\tilde{p}_i$ and $\tilde{q}_j$ are respectively the i^{th} and j^{th} columns of $\tilde{P}$ and $\tilde{Q}$. The vectorization of $\tilde{P}X\tilde{Q}$ can be expressed as:

$$\mathrm{vec}(\tilde{P}X\tilde{Q}) = \begin{bmatrix}\tilde{P}_1 \otimes \tilde{Q}_1^T & \tilde{P}_2 \otimes \tilde{Q}_2^T & \cdots & \tilde{P}_{\tilde{n}} \otimes \tilde{Q}_{\tilde{n}}^T\end{bmatrix} \begin{pmatrix} x_1 \\ x_2 \\ \vdots \\ x_{\tilde{n}} \end{pmatrix}.$$

The above two equations complete the proof of this lemma.